A theoretical study of H_2 dissociation on $(\sqrt{3}\times\sqrt{3})R30°$ CO/Ru(0001)

I. M. N. Groot,[1,2,a)] J. C. Juanes-Marcos,[1] R. A. Olsen,[1,3] and G. J. Kroes[1]
[1]*Leiden Institute of Chemistry, Leiden University, P.O. Box 9502, 2300 RA Leiden, The Netherlands*
[2]*FOM Institute for Plasma Physics Rijnhuizen, P.O. Box 1207, 3430 BE Nieuwegein, The Netherlands*
[3]*Akershus University College, P.O. Box 423, N-2001 Lillestrøm, Norway*

(Received 16 June 2009; accepted 25 February 2010; published online 13 April 2010)

We have studied the influence of preadsorbed CO on the dissociative adsorption of H_2 on Ru(0001) with density functional theory calculations. For a coverage of 1/3 ML CO, we investigated different possible reaction paths for hydrogen dissociation using nudged elastic band and adaptive nudged elastic band calculations. One reaction path was studied in detail through an energy decomposition and molecular orbital type of analysis. The minimum barrier for H_2 dissociation is found to be 0.29 eV. At the barrier the H–H bond is hardly stretched. Behind this barrier a molecular chemisorption minimum is present. Next, the molecule overcomes a second barrier, with a second local chemisorption minimum behind it. To finally dissociate to chemisorbed atoms, the molecule has to overcome a third barrier. To move along the reaction path from reactants to products, the hydrogen molecule needs to rotate, and to significantly change its center-of-mass position. The procedure of mapping out reaction paths for H_2 reacting on low-index surfaces of bare metals (computing two-dimensional elbow plots for fixed impact high-symmetry sites and H_2 orientations parallel to the surface) does not work for H_2+CO/Ru. The first barrier in the path is recovered, but the features of the subsequent stretch to the dissociative chemisorption minimum are not captured, because the molecule is not allowed to change its center-of-mass position or to rotate. The dissociative chemisorption of H_2 on CO/Ru(0001) is endoergic, in contrast to the case of H_2 on bare Ru(0001). The zero-point energy corrected energies of molecularly and dissociatively chemisorbed H_2 are very close, suggesting that it may be possible to detect molecularly chemisorbed H_2 on $(\sqrt{3}\times\sqrt{3})R30°$ CO/Ru(0001). The presence of CO on the surface increases the barrier height to dissociation compared with bare Ru(0001). Based on an energy decomposition and molecular orbital analysis we attribute the increase in the barrier height mainly to an occupied-occupied interaction between the bonding H_2 σ_g orbital and the (surface-hybridized) CO 1π orbitals, i.e., to site blocking. There is a small repulsive contribution to the barrier from the interaction between the H_2 molecule and the Ru part of the CO covered Ru surface, but it is smaller than one might expect based on the calculations of H_2 interacting with a clean Ru surface, and on calculations of H_2 interacting with the CO overlayer only. Actually, the analysis suggests that the Ru surface as a subsystem is (slightly) *more* reactive for the reaction path studied *with* CO preadsorbed on it than *without* it. Thus, the results indicate that the influence of CO on H_2 dissociation on Ru is not only a simple site-blocking effect, the electronic structure of the underlying Ru is changed. © *2010 American Institute of Physics*. [doi:10.1063/1.3378278]

I. INTRODUCTION

A very important type of heterogeneous catalysis involves the interaction of gas phase molecules with solid surfaces. This interaction can lead to reflection of the molecules back into the gas phase or (dissociative) adsorption of the molecules, possibly followed by a chemical reaction between different adsorbates. One of the processes investigated in great detail is the dissociative adsorption of hydrogen on different metal surfaces (for reviews, see Refs. 1–5), which has been recognized as an elementary step in many industrial processes, e.g., the production of ammonia.[6]

To get more insight into chemical reactions occurring at surfaces, the coadsorption of hydrogen and different other adsorbates has also been studied (see, e.g., Refs. 7–26). Examples of these studies involve the so-called "poisoning" of hydrogen dissociation on Pt(533) by O_2,[23] on Pt(111) by K,[14] on Ni(100) by S,[8–11] on Pd(111) by S and Cl,[21] on Pd(100) by S,[11,12,15,17–20,22] and on Ru(0001) by S.[7] Different effects of poisoning can be observed: Dissociation sites for hydrogen can be completely blocked by the adsorbate at the experimentally relevant conditions, additional energy barriers can be built up along the dissociation pathway of hydrogen, and the heights of energy barriers can be changed. Theoretical studies on H_2+S/Pd(100) claim that the poisoning gives rise to the build-up of energy barriers on the potential energy surface (PES),[15,17–20,22] while experiments on the same system observed site-blocking effects.[12] Experiments of D_2 dissociation on CO/Ru(0001) observe both effects.[27] Possible

a)Present address: Fritz-Haber-Institut der Max-Planck-Gesellschaft, Faradayweg 4-6, 14195 Berlin, Germany. Electronic mail: groot@chem.leidenuniv.nl.

poisoning mechanisms include a change in the density of states at the Fermi level[28–30] and an adlayer induced electrostatic field.[31,32]

The poisoning of hydrogen adsorption by CO on different metal surfaces has also been studied under high pressure conditions.[33] The authors find an H–D exchange rate that varies more strongly with CO coverage than would be expected from a simple site-blocking mechanism. The addition of 10 ppm CO has a significant effect on the reaction probability of H_2. The metal most sensitive to this influence is Ir, followed by Pt. Palladium is found to be the least sensitive to the presence of CO. The process investigated in this paper, the dissociative adsorption of H_2 on CO-precovered Ru(0001), is particularly interesting for the methanation reaction,[34–37] and for Fischer–Tropsch synthesis.[38–40]

The individual adsorption of CO and H_2 on Ru(0001) has been studied in detail. Carbon monoxide adsorbs nondissociatively,[41–44] preferentially at the on-top position for coverages up to 1/3 ML, oriented perpendicular to the surface.[45–49] The C-end is bound to the surface, with the O atom facing the vacuum.[41,50,51] Different experimental low-energy electron diffraction (LEED) structures have been found for several coverages of CO. At 1/3 ML a $(\sqrt{3}\times\sqrt{3})$R30° structure is observed.[45,52–54] At 1/2 ML, a $(2\sqrt{3}\times2\sqrt{3})$R30° structure is assigned, with either equal populations of top, hcp hollow and fcc hollow sites,[55] or exclusively top sites.[56] A $(2\sqrt{3}\times2\sqrt{3})$R30° structure has also been observed at 7/12 ML.[52,55] A saturated $(5\sqrt{3}\times5\sqrt{3})$R30° structure (assigned coverage of 49/75 ML) was observed by LEED (Ref. 52) and helium scattering experiments.[57] For coverages below 1/3 ML, a lattice gas in equilibrium with $(2\sqrt{3}\times2\sqrt{3})$R30° islands is observed.[54]

Molecular hydrogen adsorbs dissociatively on the Ru(0001) surface, and the H atoms bind preferentially in the fcc hollow sites.[58] Both experiment[59,60] and theory[61] observe direct, activated adsorption, with a suggestion of nonactivated adsorption occurring at low collision energies in experiment.[59,60] No isotope effect is seen over a wide range of kinetic energies, and normal energy scaling is obeyed.[60] The saturation coverage equals 1 ML with respect to the Ru surface atoms.[62]

The coadsorption of hydrogen and CO on Ru(0001) has been studied both experimentally[27,33,57,63–67] and theoretically.[42,65] The interaction between CO and H/D is repulsive, as is found from temperature programmed desorption,[67] He atom scattering,[57] thermal energy He atom scattering,[67] and density functional theory (DFT) studies.[65] No chemical reaction between CO and H/D was found.[63]

In this paper, we present a study of different possible hydrogen dissociation pathways at the CO-precovered Ru(0001) surface. By using (adaptive) nudged elastic band calculations we find the barrier geometries for the reaction path in which all six degrees of freedom of the H_2 molecule have been optimized. In addition, we present two-dimensional (2D) (r,Z) cuts through the six-dimensional (6D) PES for fixed center-of-mass (COM) positions and orientations of H_2 parallel to the surface. The reaction path of hydrogen dissociation is studied in more detail by two-center projected density of states (PDOS) calculations and an energy decomposition analysis.

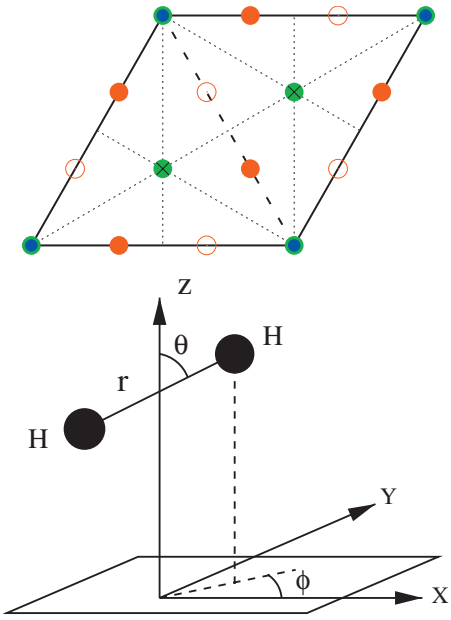

FIG. 1. (Top panel) A schematic top view of the $(\sqrt{3}\times\sqrt{3})$R30° unit cell used to model the CO/Ru(0001) surface. The length of the unit cell is $\sqrt{3}a$=4.75 Å. The dark blue circles represent CO molecules adsorbed perpendicular to the surface. The green and red circles represent Ru atoms in the first (top) and second (hcp) layers, respectively. The open red circles represent fcc sites. Only the top two Ru layers are shown. In the structure of Ru(0001), the third layer is directly below the first layer. The mirror plane is indicated by a black, dashed thick line and the threefold rotation axes are indicated by black crosses. The dotted lines indicate planes which act as symmetry planes in the approximation that the H_2 interaction with fcc sites is equal to its interaction with hcp sites. (Bottom panel) The 6D (X,Y,Z,r,θ,φ) coordinate system used to describe the interaction of H_2 with the CO/Ru(0001) surface. For simplicity the CO molecules and Ru atoms are not explicitly shown. The *x*-axis is takes as the bottom line in the top panel going from CO to an hcp site.

The rest of the paper is organized as follows. Section II describes the details of the computational methods used. Results are given and discussed in Sec. III. Finally, Sec. IV summarizes our main conclusions.

II. THEORY

A. H_2+CO/Ru(0001) system

For carbon monoxide adsorbed on the Ru(0001) surface, a coverage of 1/3 ML is considered, with the CO molecules bound at the on-top sites, perpendicularly to the surface with the C atom closest to it. A $(\sqrt{3}\times\sqrt{3})$R30° surface unit cell is used, as this is the structure experimentally seen by LEED of 1/3 ML CO on Ru(0001).[45,52–54] A schematic top view of the unit cell is shown in Fig. 1 (top panel). Note that the unit cell contains two threefold rotational axes and a mirror plane, as indicated in the figure. As a result, in our calculations each H_2+CO/Ru(0001) configuration has five symmetry equivalent configurations. Two of these are related to the original configuration by a rotation of H_2 along one of the two threefold rotation axes, by 120° and 240°, respectively. The other three can be obtained from the three configurations generated in this way by reflecting H_2 in the symmetry plane of Fig. 1.

In addition, six configurations are closely related to the six symmetry equivalent ones generated as discussed above. In Fig. 1 (top panel), the six planes perpendicular to the figure and indicated by the dotted lines almost act as mirror planes, because to a good approximation the interaction of H_2 with a Ru fcc site is equal to that with a Ru hcp site. Thus, we say that the six additional configurations generated by reflecting the six true symmetry equivalent ones in these planes are related to these by a "symmetry near equivalence."

Based on the top panel of Fig. 1, we may already speculate on the effect of CO adsorption on the H_2 dissociation in the system studied. The CO is blocking 1/3 of the top (surface atoms) Ru sites, which have the lowest barrier to H_2 dissociation on bare Ru(0001).[61,68] This should lower the reaction probability. In addition, all preferred atomic chemisorption sites (the fcc sites[58]) are close to adsorbed CO molecules, the distance being 1.58 Å. As we will see below, this complicates H_2 dissociation relative to that on the bare Ru(0001) surface, by introducing additional barriers in the reaction path.

The H_2 molecular configuration is described by the six coordinates X, Y, Z, r, θ, and φ. Here, r is the H–H distance, Z is the distance from the COM of H_2 to the surface, X and Y represent the COM motion parallel to the surface, and θ and φ are the polar and azimuthal angles defining the orientation of the H–H molecular axis. This coordinate system is displayed in Fig. 1 (bottom panel).

B. Electronic structure calculations

The electronic structure calculations are done applying DFT[69,70] as implemented in the DACAPO code.[71] The exchange-correlation functional is described within the generalized gradient approximation (GGA), using a revised Perdew–Burke–Ernzerhof (RPBE) functional.[72] This functional is known to give rather accurate chemisorption energies for CO on a range of flat metal surfaces, including Ru(0001).[73] Comparison of experiment[60] to earlier predictive 6D quantum dynamics calculations[61] suggests that the PW91 functional[74] overestimates the reactivity of H_2 on Ru(0001), whereas the RPBE functional underestimates it. The same result has recently been obtained for H_2+Cu(111).[75] There is no systematic proof yet that other standard GGA functionals perform better for H_2-metal surface reactions, although very recent results suggest that chemically accurate results for molecular beam reaction probabilities are obtainable with a specific reaction parameter DFT approach.[75] The ionic cores are modeled using ultrasoft pseudopotentials[76] and a plane-wave basis set is used for the electronic orbitals.

The CO/Ru(0001) system is modeled using a three-layer slab of Ru-atoms and a $(\sqrt{3}\times\sqrt{3})$R30° surface unit cell. To check whether the relatively small amount of three layers in the Ru slab is enough, we calculated the height of the dissociation barrier for slabs with three to nine layers of Ru atoms. The difference in barrier height between the lowest and highest value calculated is 0.016 eV. This difference is small enough that the number of three layers is acceptable. To avoid artifacts caused by the use of periodic boundary conditions along Z, we placed a vacuum layer of 15 Å between the slabs in this direction (the vacuum distance being defined as the distance from the O-atom of adsorbed CO to the bottom of the periodic image of the Ru slab). The total height of the unit cell is thus 22.3 Å, and the distance between the top of the Ru slab and the bottom of its periodic image is 18.1 Å. The Brillouin zone is sampled by a set of (8,8,1) Monkhorst–Pack k-points.[77] The kinetic energy cutoff of the plane wave basis used for the electronic orbitals is set at 400 eV, whereas an 800 eV cutoff is used for the density grid. The electronic smearing energy we use is 0.1 eV and the calculations are performed spin-unpolarized. It was checked whether spin-polarized calculations were necessary, but no significant difference was observed when comparing these to the results of spin-unpolarized calculations.

All Ru atoms and the CO adsorbate are taken as frozen, after allowing the atoms to relax in the Z-direction. This approximation would seem to be reasonable for the following two reasons: First, reaction probabilities measured in molecular beam experiments on H_2+Ru(0001) (Ref. 60) and H_2+CO/Ru(0001) (Ref. 27) show no dependence on surface temperature. Second, it seems reasonable to assume that the heavier, and therefore slower CO molecule, would not have sufficient time to move out of the way of the lighter, faster moving H_2 molecule. For the clean Ru(0001) slab a relaxed interlayer distance of 2.12 Å was found for both the distance between layers 1 and 2, and between layers 2 and 3, compared with 2.18 Å for bulk Ru.[61] For the lattice parameter a we use a=2.745 Å. The Ru interlayer distance was relaxed using the quasi-Newton method in the presence of relaxed CO and a value of 2.11 Å was obtained for both layers, which is slightly compressed with respect to the Ru slab without CO present (2.12 Å). The Ru atoms on which the CO molecules reside are slightly lifted from the surface, by 0.11 Å. This agrees with earlier calculations done with the VASP code and the PW91 functional.[49]

The CO molecule is found to be nondissociatively adsorbed perpendicular to the surface, as was found previously both theoretically[42–44] and experimentally.[41] The C-end is attached to the Ru atom, and the calculated C–Ru distance is 1.93 Å. The C–O distance we find is 1.18 Å, compared with 1.16 Å for the gas phase. These values compare well to other calculations[42,44,47–49] and experimental results[45,78] (see Table I). Several high-symmetry adsorption sites were explored for CO on the Ru(0001) surface. The adsorption energy is defined as $E_{ads}=E_{CO}+E_{Ru}-E_{CO/Ru}$. The on-top site is found to be the most stable adsorption site with an adsorption energy of 1.85 eV, comparing well to earlier calculations[42,47,80,81] and experiments,[81–83] with experimental results ranging from 1.49 to 1.81 eV. Assuming that the most recent experimental value [1.49 eV (Ref. 81)] of the adsorption energy is the most accurate one, our theoretical RPBE result (1.85 eV) overestimates the adsorption energy, in accordance with the observation that this GGA still overbinds for molecule-metal surface interactions.[72] For the other high-symmetry sites we find the following adsorption energies: 1.66 eV for the bridge site, 1.65 eV for the hcp hollow site, and 1.57 eV for the fcc hollow site. For an overview of our results and results from the literature, see Table I.

TABLE I. Overview of our results and results from literature for the C–Ru, and the C–O distance, and the absolute value of the adsorption energy E_{ads} for different CO adsorption sites. Distances are in angstrom and energies in eV. T=theory and E=experiment.

Reference	Adsorption site	C–Ru	C–O	E_{ads}	T/E	Functional
This paper	Top	1.93	1.18	1.85	T	RPBE
	Bridge			1.66	T	RPBE
	hcp hollow			1.65	T	RPBE
	fcc hollow			1.57	T	RPBE
Stroppa 2008[a]	Top			1.99	T	PBE
				2.14	T	HSE
				1.50	T	BLYP
				1.78	T	B3LYP
	fcc hollow			1.82	T	PBE
				1.77	T	HSE
				1.08	T	BLYP
				1.17	T	B3LYP
McEwen 2007[b]	Top	1.894	1.165		T	PW91
Gajdos 2004[c]	Top	2.03	1.166		T	PZ
Ciobica 2003[d]	Top			1.96	T	PW91
	Bridge			1.72	T	PW91
	hcp hollow			1.83	T	PW91
	fcc hollow			1.76	T	PW91
Ciobica 2003[e]	Top	1.90	1.17	1.81	T	PW91
Christoffersen 2002[f]				1.65	T	RPBE
Mortensen 1997[g]	Top	1.92	1.17	1.90	T	PW91
	Bridge			1.70	T	PW91
	hcp hollow			1.78	T	PW91
Hammer 1996[h]	Top			1.80	T	PW91
Abild-Pedersen 2007[i]	Top			1.49 ± 0.22	E	
Over 1993[j]	Top	1.93 ± 0.04	1.10 ± 0.05		E	
Michalk 1983[k]	Top	2.00 ± 0.1	1.10 ± 0.10		E	
Pfnür 1983[l]	Top			1.81	E	
Pfnür 1978[m]	Top			1.66	E	

[a]Reference 79.
[b]Reference 49.
[c]Reference 44.
[d]Reference 43.
[e]Reference 42.
[f]Reference 73.
[g]Reference 47.
[h]Reference 80.
[i]Reference 81.
[j]Reference 78.
[k]Reference 45.
[l]References 83.
[m]Reference 82.

C. Locating barriers along different H_2 dissociation paths

Different H_2+CO/Ru(0001) reaction paths and the corresponding barrier heights and transition states were determined. By a reaction path we mean a path from hydrogen in the gas phase to two H atoms chemisorbed atomically on the surface, and proceeding through stationary points. Reaction paths were determined using two different methods: (i) adaptive nudged elastic band (ANEB) (Ref. 84) calculations where the hydrogen molecule is free to move in all six degrees of freedom, but the CO molecule and surface Ru atoms are kept frozen; and (ii) determination of (further) constrained minimum energy paths in 2D cuts through the full 6D PES by exploring the two coordinates r and Z, and (additionally) fixing the remaining ones (X, Y, θ, φ). We studied four different constrained reaction paths in which we chose the H_2–Ru geometries to be the same as were studied for H_2 dissociation on bare Ru(0001),[68] i.e., with the COM of H_2 on top of a bare Ru atom, in the bridge position, in the hcp site and between the top and fcc site (t2f), respectively, and H_2 oriented parallel to the surface. To obtain the 2D (r,Z) cuts single point DFT calculations were done for seven different values of r and 13 different values of Z. The results were interpolated using cubic splines and the energy barriers were found from the 2D spline fits.

The ANEB calculations are done in the following way. For different high-symmetry sites of an H atom at the CO/Ru(0001) surface, the relaxed energy minimum is calculated using the quasi-Newton method. For the configuration with the lowest energy a second H atom at a high-symmetry site is added and again the energy is minimized. This is done for four different configurations. These four configurations are used as the final configurations (two chemisorbed atoms) in four calculations with the ANEB method. The initial configuration (H_2 in gas phase) is then calculated by using the same COM X and Y coordinates as used in the initial geometries employed to compute the geometry and energy of the dissociated molecule (which had both H atoms in a high-symmetry site), but with a bond length r=0.75 Å, and a height Z (8.45 Å) that corresponds to a molecule-surface

distance where the molecule-surface interaction is negligible. Three images are linearly interpolated and equally spaced between the initial and final configurations. Between adjacent images, artificial spring forces are added, in order to keep the images equally spaced along the band. The images are moved by minimizing with the quasi-Newton method both the real force acting on them perpendicular to the band, and the artificial spring force parallel to the band. The barrier is found by taking the two images around the local maximum as the new initial and final configurations, and applying the same procedure iteratively until no more significant changes in the maximum are found. The highest energy image gives then a good estimate of the transition state.

The studied reaction paths were explored in additional detail using the NEB method to refine stretches of the reaction path. The initial and final configurations used were the same as in one of the ANEB calculations. Then ten images were linearly interpolated and equally spaced in between. These ten configurations were moved applying the same method described above for the ANEB calculations. These calculations were performed to verify the existence of additional saddle points. We also performed additional energy minimizations to characterize local minima in the reaction paths.

D. Two-center projected density of states calculations

We calculate the two-center PDOS for several H_2 configurations along the reaction path studied by NEB. Together with an energy decomposition analysis it is then possible to develop a molecular orbital based description of the repulsive and attractive interactions, and thereby obtain a qualitative understanding of the dissociation mechanism of H_2 on CO/Ru(0001).

The two-center PDOS is calculated at energies ϵ of the localized orbital ϕ_a as

$$n_a(\epsilon) = \sum_i \sum_k |\langle \phi_a | \psi_{ik} \rangle|^2 \delta(\epsilon - \epsilon_{ik}), \tag{1}$$

where i runs over all electronic bands, and k labels the k-points used for sampling the Brillouin zone. The ψ_{ik} are the Kohn–Sham wave functions and the ϵ_{ik} are the corresponding energies. The Fermi level is set to zero on the energy scale. The δ-function is represented by a Gaussian function with a width of 0.1 eV. In Eq. (1) ϕ_a was chosen as either the H_2 molecular bonding (σ_g) or antibonding (σ_u) orbital, which are constructed by the normalized linear combinations of hydrogen s orbitals, ϕ_s^H, centered at the positions of the two H atoms $\mathbf{R}_1$ and $\mathbf{R}_2$

$$\begin{aligned} \phi_{\sigma_g}(\mathbf{r}) &= c_1\{\phi_s^H(\mathbf{r}-\mathbf{R}_1) + \phi_s^H(\mathbf{r}-\mathbf{R}_2)\}, \\ \phi_{\sigma_u}(\mathbf{r}) &= c_2\{\phi_s^H(\mathbf{r}-\mathbf{R}_1) - \phi_s^H(\mathbf{r}-\mathbf{R}_2)\}. \end{aligned} \tag{2}$$

Here $c_1 = 1/\sqrt{2(1+S)}$ and $c_2 = 1/\sqrt{2(1-S)}$ are the normalization coefficients. Furthermore, S is the overlap term given by $S = \int \phi_s^{H*}(\mathbf{r}-\mathbf{R}_1)\phi_s^H(\mathbf{r}-\mathbf{R}_2)d\tau$, which is analytically calculated by[85]

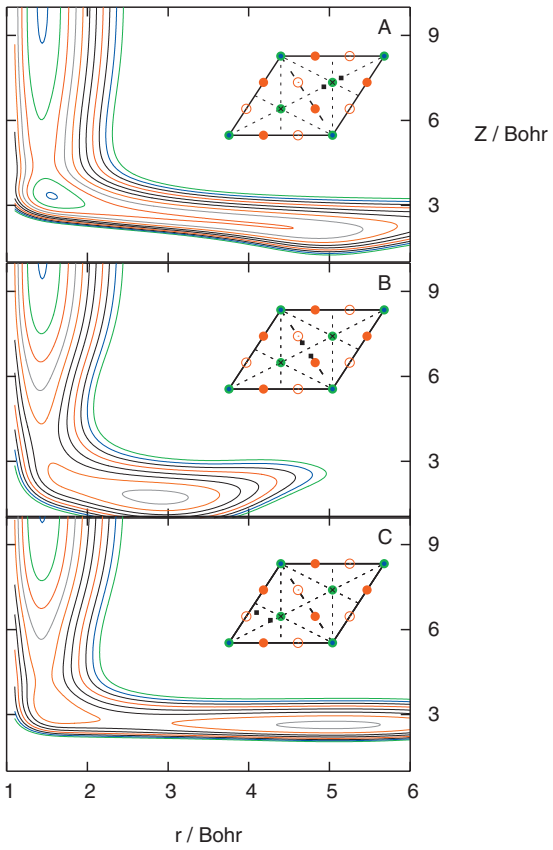

FIG. 2. 2D cuts through the PES, with the COM above (a) the top site; (b) the bridge site; and (c) the t2f site. The zero of the potential energy scale is the gas phase minimum energy. The contours have a spacing of 0.2 eV, and the first contour occurring near 1.4 bohr at large Z is the 0 eV contour. The insets show the position and orientation of H_2, the orientation being parallel to the surface.

$$S = \left\{ 1 + \frac{|\mathbf{R}_1 - \mathbf{R}_2|}{a_0} + \frac{1}{3}\left(\frac{|\mathbf{R}_1 - \mathbf{R}_2|}{a_0} \right)^2 \right\} \times \exp(-|\mathbf{R}_1 - \mathbf{R}_2|/a_0), \tag{3}$$

where a_0 is the Bohr radius.

III. RESULTS AND DISCUSSION

A. Barrier heights and locations

Figure 2 shows elbow plots for three of the four dissociation geometries studied, i.e., the top site, the bridge site, and the t2f site. For the geometry where the COM of the H_2 molecule is placed above the hcp site, very high energies are found, indicating that this is not a favorable route to dissociation. This observation is explained by the fact that above the hcp site, the H_2 molecule is close to a CO molecule. For the other three geometries a barrier and a molecular chemisorption well are observed. For the top and bridge geometries the molecule-surface interaction energy keeps increasing along the minimum energy path (MEP) with further stretching of the H–H distance, after the molecular chemisorption well is passed.

For the t2f reaction path [Fig. 2(c)], a second barrier and well are observed. After the second well is passed, the molecule-surface interaction energy increases along the MEP

TABLE II. Barrier heights, well depths, and locations for the dissociation of H_2 parallel to the surface for the three constrained adsorption geometries considered, taking the energy of H_2 in the gas phase as zero. The results for bare Ru(0001) are taken from Ref. 68. The subscripts "b" and "w" labeling energies and coordinates refer to barriers and wells, respectively. The φ values provided for the bare Ru(0001) system are here taken relative to the coordinate system defined in Fig. 1.

	Top bare	Top CO/Ru	t2f bare	t2f CO/Ru	Bridge bare	Bridge CO/Ru
E_b^1/eV	0.085	0.30	0.18	0.74	0.33	0.85
Z_b^1/Å	2.58	2.40	2.27	2.26	1.98	1.92
r_b^1/Å	0.77	0.77	0.78	0.77	0.80	0.78
φ/deg	30	30	148	148	120	120
E_w^1/eV		0.05		0.65		0.55
Z_w^1/Å		1.55		1.70		0.93
r_w^1/Å		0.82		0.83		1.50
E_b^2/eV				0.84		
Z_b^2/Å				1.46		
r_b^2/Å				1.34		
E_w^2/eV				0.55		
Z_w^2/Å				1.40		
r_w^2/Å				2.65		

upon further stretching of the H–H bond. Table II gives an overview of the barrier heights and geometries and well depths and geometries for these reaction paths, as well as the barrier heights and geometries for bare Ru(0001). When comparing the barrier heights of bare and CO-precovered Ru, it is immediately clear that the presence of CO on the surface significantly increases the barrier height. The trend in barrier height is the same for the two systems: Above the top site the barrier is lowest, followed by the t2f site, and the bridge site. Furthermore, the barriers occur at approximately the same geometries (r and Z values) for CO/Ru as for bare Ru(0001). Finally, it is also clear that the constrained 2D reaction paths studied here do not yield dissociative chemisorption minima. For that, it is also necessary to allow the H_2 COM to move away from the site at which the lowest barrier to molecular chemisorption occurs, as we will now show.

Four reaction paths with the COM of the H_2 molecule initially at or close to the CO "hollow" sites, i.e., on top of a free Ru atom (green circle with cross on it in Fig. 1), were investigated in detail by ANEB calculations, which put no constraint on the intermediate values of X, Y, θ, and φ. Additionally, we further investigate stretches of one of these reaction paths with nudged elastic band calculations, as described in Sec. II C. By studying the four reaction paths in detail, and taking into account the symmetry equivalence and near equivalence of specific geometries (see Sec. II A), it turns out that the four reaction paths studied below show essentially the same barriers and (molecular) chemisorption wells. Here, we discuss one reaction path in detail (reaction path I). See supplementary material document for details of the other three reaction paths (reaction paths II-IV).[86]

The reaction path shows a complex energy landscape, with more than one barrier and minimum present. Figure 3 shows the plot of the energy versus the reaction coordinate for reaction path I. The energy of the gas phase is taken as zero and the reaction coordinate is defined as

$$R_i = \sum_0^i \sqrt{(X_i - X_0)^2 + (Y_i - Y_0)^2 + (Z_i - Z_0)^2 + (r_i - r_0)^2}, \tag{4}$$

where "0" corresponds to the gas phase configuration.

From this figure, we observe a barrier (labeled "1" in Fig. 3) with a height of 0.29 eV (all energies quoted are relative to H_2+CO/Ru, with H_2 in the gas phase). In addition, we observe a local molecular chemisorption minimum with an energy of 0.074 eV (labeled "2" in Fig. 3). Here, the H–H distance is only 0.85 Å, hardly larger than the gas phase H–H bond distance of 0.75 Å. When proceeding along the reaction coordinate, we then observe a second, lower barrier, of 0.24 eV (labeled "3" in Fig. 3). Behind this barrier, a second, local chemisorption minimum with an energy of 0.19 eV is observed (labeled "4" in Fig. 3), followed by another barrier of 0.23 eV (labeled "5"). Finally the molecule moves to the dissociated chemisorption minimum with an energy of 0.10 eV (labeled "6" in Fig. 3).

Since the final state (labeled 6 in Fig. 3) has a higher

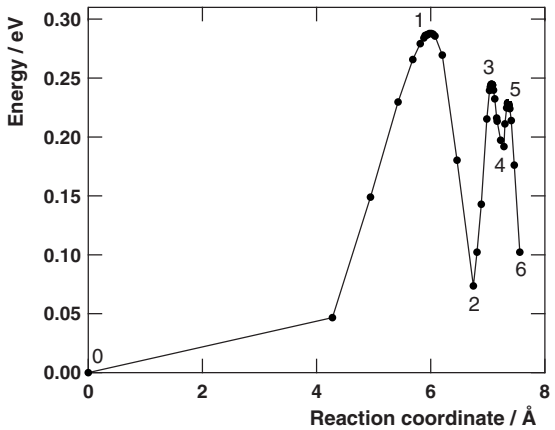

FIG. 3. Energy vs reaction coordinate for the reaction path studied by ANEB calculations. The energy of H_2 in the gas phase is taken to be zero, and the definition of the reaction coordinate is given in the text [see Eq. (4)].

TABLE III. Frequencies of molecularly adsorbed H_2 on CO/Ru(0001) and the character of the normal modes. A "combination" mode is a combination of the motion where the COM of the molecule vibrates parallel to the surface and of the "helicopter" rotation of the molecule (rotation in a plane parallel to the surface).

Frequency (cm^{-1})	Character vibration
3027	H–H stretch
1569	Hindered cartwheel rotation
804	Perpendicular molecule-surface stretch vibration
462	Combination
426	Combination
339	Combination

energy than the molecular chemisorption minimum (labeled 2 in Fig. 3, 0.10 eV versus 0.07 eV), one could wonder whether the hydrogen molecule actually dissociates. However, to compare these energies, the zero-point energy of both configurations has to be taken into account. For configuration 2, we calculate a zero-point energy of 0.41 eV, indicating that this configuration has a total energy of 0.41 +0.07=0.48 eV. For configuration 6 this calculation results in a zero-point energy of 0.34 eV, and a total energy of 0.34+0.10=0.44 eV. This calculation shows that the final configuration has a somewhat lower total energy, making it likely that the H_2 molecule will indeed fully dissociate.

However, the fact that these energies lie so close, may indicate that molecularly chemisorbed H_2 will be present on the CO/Ru(0001) surface. A possible experimental technique to observe molecularly chemisorbed hydrogen on the surface, is electron energy loss spectroscopy. With this technique, molecularly adsorbed H_2 was observed on the stepped Cu(510) surface for very low surface temperatures (10–20 K).[87] Perhaps this technique can also be used to search for molecular H_2 on CO/Ru. To facilitate the search for molecularly adsorbed H_2 on CO/Ru(0001), the frequencies of the normal modes of molecularly adsorbed H_2 calculated by diagonalizing the Hessian matrix are gathered in Table III.

The dissociation described by the reaction path is endoergic. The energy of the final state lies above 0, the energy of the gas phase. This is in contrast with H_2 dissociation on bare Ru(0001), which is observed to be exoergic.[68] Hence, the endoergicity must be caused by the presence of the CO molecules.

For the configurations discussed above, the positions of the separate H atoms in the unit cell are shown in Fig. 4. The initial (0 in Fig. 3), first barrier (1 in Fig. 3) and first molecular chemisorption configuration (2 in Fig. 3) are all on top of a bare Ru atom, and the H–H bond is hardly stretched in these configurations. In the reaction path, at the barrier to molecular chemisorption (1 in Fig. 3), the COM is thus at the same impact site for which the lowest barrier to molecular chemisorption is found in the constrained 2D reaction paths [see Fig. 2(a)], and in the same position for which the lowest barrier is found for dissociative chemisorption of H_2 on bare Ru(0001).[68] The H–H bond starts to stretch and the molecule's COM moves away from the top site when one of the H atoms moves away from the top position toward the most

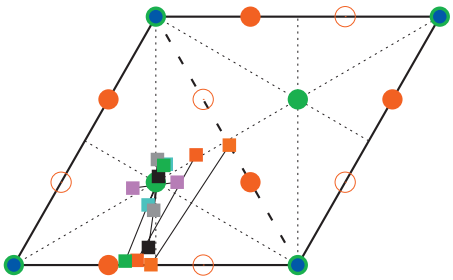

FIG. 4. For the reaction path studied by ANEB calculations the positions of the hydrogen atoms in the initial state (pink, 0 in Fig. 3), in the first barrier configuration (light blue, 1 in Fig. 3), in the molecular chemisorption minimum (gray, 2 in Fig. 3), in the second barrier configuration (black, 3 in Fig. 3), in the second chemisorption minimum (green, 4 in Fig. 3), in the third barrier configuration (red, 5 in Fig. 3), and in the final state (orange, 6 in Fig. 3) are shown in the CO/Ru(0001) unit cell. The CO molecules and Ru atoms are displayed as in Fig. 1.

favorable atomic chemisorption site on bare Ru(0001), i.e., an hcp site. This movement gives rise to a second, lower barrier (black configuration in Fig. 4, and 3 in Fig. 3). Next, the H atom moves further toward the hcp site, creating a local chemisorption minimum (green configuration, 4 in Fig. 3). Then the second H atom moves away from the top site on its way to another hcp site, giving rise to the barrier labeled 5 in Fig. 3 (red configuration in Fig. 4). Finally, the molecule is dissociated with both atoms close to neighboring hcp sites (orange configuration, 6 in Fig. 3). Now the H atoms are 2.38 Å apart. In the final geometry the H atoms are displaced from the hcp sites to minimize their interaction with CO. For all seven configurations discussed above the positions and energies are given in Table IV.

It is illuminating to compare the reaction paths computed here for H_2+CO/Ru to that for H_2+bare Ru(0001).[68] For the bare system, the dissociation takes place above the top site. The reaction path shows one barrier, at essentially the same geometry as the barrier to molecular chemisorption in H_2 +CO/Ru. After crossing this barrier on bare Ru, the COM stays above the top site, while one H atom moves to an hcp site and the other to an fcc site. On CO/Ru, the hcp and fcc sites themselves are blocked by the presence of nearby CO. In order to move to the most favorable atomic chemisorption sites, which are somewhat removed from the hcp sites, the molecule's COM has to move away from the top site. In the ANEB analysis, it does so in two steps, to allow the H atoms to move to their favored atomic chemisorption sites sequentially.

Having found the true saddle points through the ANEB analysis, we may now evaluate the usefulness of the strategy used to find reaction paths for H_2+bare Ru(0001) to determine reaction paths for H_2+CO/Ru, by evaluating 2D elbow potentials for impact on high-symmetry sites at fixed H_2 positions parallel to the surface. This strategy yields a good estimate of the lowest barrier height and geometry for molecular chemisorption of H_2 on CO/Ru (0.30 eV, r=0.77 Å, and Z=2.40 Å according to the 2D analysis, see Table II, and 0.29 eV, r=0.76 Å, and Z=2.44 Å from the ANEB analysis, Table IV). However, the 2D constrained approach fails to uncover the dissociative chemisorption minimum and the intermediate barriers and chemisorption minima. It can-

TABLE IV. Positions, reaction coordinates, and energies of the seven configurations discussed for the reaction path studied with ANEB calculations. $z=0$ is defined as the average z-coordinate of the first layer Ru atoms. The energy of H_2 in the gas phase is taken as zero. The definition of the reaction coordinate is given in Eq. (4). The numbers added to the description of the configuration correspond to the numbers of the points in the reaction path displayed in Fig. 3.

Configuration	X (Å)	Y (Å)	r (Å)	Z (Å)	θ (deg)	φ (deg)	R (Å)	Energy (eV)
Gas phase (0)	2.36	1.32	0.75	8.45	90	8	0.00	0.00
First barrier (1)	2.40	1.34	0.76	2.44	102	66	6.01	0.29
First chemisorption minimum (2)	2.37	1.33	0.85	1.70	91	86	6.75	0.07
Second barrier (3)	2.34	0.88	1.26	1.41	107	82	7.07	0.24
Second chemisorption minimum (4)	2.19	0.86	1.81	1.26	108	68	7.28	0.19
Third barrier (5)	2.56	0.95	2.03	1.22	99	60	7.36	0.23
Atomic chemisorption minimum (6)	2.95	1.00	2.38	1.10	90	56	7.56	0.10

not be used to map out the complete reaction path because the COM of the molecule is kept fixed, thereby hindering the consecutive motions of the two H atoms from their initial positions in the molecular chemisorption well to their preferred atomic chemisorption sites.

B. An energy decomposition and a molecular orbital analysis of the H_2 approach to the surface and the subsequent dissociation

To understand the mechanism of H_2 dissociation on CO-precovered Ru(0001) stretches of a near symmetry equivalent reaction path to path I (i.e., reaction path II in the supplementary material[86]) were studied in more detail by NEB calculations (see Sec. II C). The coordinates of six selected configurations along this path are given in Table V. Figure 5 shows a visualization of these 6 configurations. We observe that the H_2 molecule rotates to achieve a geometry that closely corresponds to the first barrier (orange configuration in Fig. 5) and to the molecular chemisorption minimum (black configuration). Along this path two-center PDOS calculations are done for the total system and three subsystems: H_2 with preadsorbed CO on the Ru surface [Figs. 6(a)–6(d)], H_2 interacting with a clean Ru surface [Figs. 6(e)–6(h)], H_2 with only the CO overlayer [Figs. 6(i)–6(l)], and H_2 only (results not shown). Figure 1 of the supporting information shows the energy landscape along the reaction coordinate for this reaction path. The configurations for which the PDOS calculations are done are indicated with arrows in this figure. The PDOS plots are shown for four of the six configurations along the reaction path given in Table V and Fig. 5 [configuration C (magenta in Fig. 5) is left out because the two-center PDOS are virtually identical to those in configuration B (green in Fig. 5), and the last configuration (F) is left out (pink in Fig. 5)]. The corresponding energy profiles are given in Table V and Fig. 7.

If the H_2 molecule is far from the surface, only the H_2 σ_g bonding state is occupied [Figs. 6(a), 6(e), and 6(i), peaks at ~ -6 eV]. It is essentially a molecular state that is slightly broadened due to the interaction with its periodic images. However, one should note that part of the broadening seen in Fig. 6 is due to the finite width used to represent the δ-function in Eq. (1).

When moving the H_2 molecule closer to the CO/Ru surface (to the configurations labeled B and C) a repulsion of 0.09 and 0.14 eV is encountered. Table V and Fig. 7 indicate this to be dominated by a direct repulsion between H_2 and CO. The repulsion is mainly due to an occupied-occupied interaction between the bonding H_2 σ_g orbital and the (surface-hybridized) CO 1π orbitals: There is virtually no change in the two-center PDOS for clean Ru when moving from the gas phase to configuration B [Figs. 6(e) and 6(f)], but a clear change is seen for the interaction with only the CO overlayer [the H_2 σ_g peak in Fig. 6(i) is seen to split in an H_2 σ_g–CO 1π bonding peak and an H_2 σ_g–CO 1π antibonding peak in Fig. 6(j)]. Thus, the change seen in Figs. 6(a) and 6(b) is dominated by the interaction with the CO overlayer, and this is fully consistent with the picture from the energy decomposition analysis. Note that the occupied-occupied repulsion between H_2 σ_g and (surface-hybridized) CO 4σ and 5σ is very small [not visible in Figs. 6(b) and

TABLE V. Coordinates and energies in eV for the H_2 molecule in six selected configurations along one reaction path for H_2 dissociation on CO-precovered Ru(0001). See text and Fig. 5. In parentheses, the configurations from Figs. 3 and 4 are given that correspond to or are close to these configurations. The H_2 gas phase energy is taken to be zero. The energies are compared for H_2+CO/Ru(0001), H_2+Ru(0001), H_2 with the CO overlayer only, and H_2 only.

Configuration	X (Å)	Y (Å)	r (Å)	Z (Å)	θ (deg)	φ (deg)	H_2+CO/Ru	H_2+Ru	H_2+CO	H_2
A gas phase (0)	2.38	1.38	0.75	8.45	90	160	0.00	0.00	0.00	0.00
B entrance channel 1	2.38	1.38	0.75	4.17	90	160	0.09	−0.01	0.11	0.00
C entrance channel 2	2.36	1.36	0.75	3.58	29	93	0.14	0.01	0.14	0.00
D barrier (1)	2.38	1.32	0.76	2.51	55	90	0.29	0.14	0.24	0.00
E first chemisorption minimum (2)	2.36	1.37	0.81	1.81	90	86	0.10	−0.14	0.26	0.06
F second chemisorption minimum (4)	2.44	0.87	1.72	1.30	73	104	0.21	−0.28	3.87	3.73

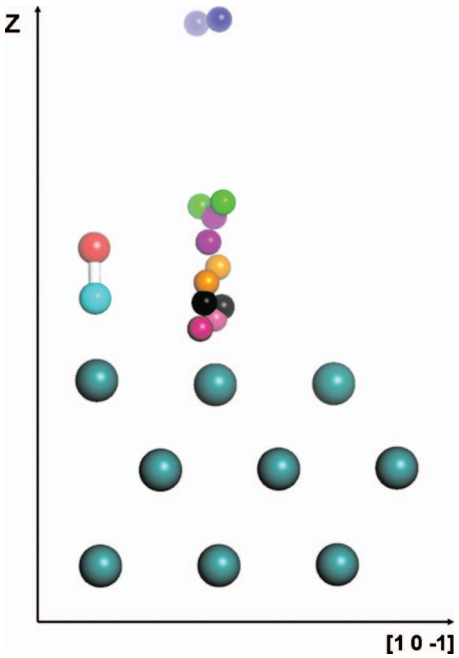

FIG. 5. Visualization of six configurations along the minimum energy reaction path for H_2+CO/Ru(0001) as found from NEB calculations. These six configurations are the same that are studied with PDOS calculations (see text for details). Blue=A, green=B, magenta=C, orange=D, black=E, and pink=F.

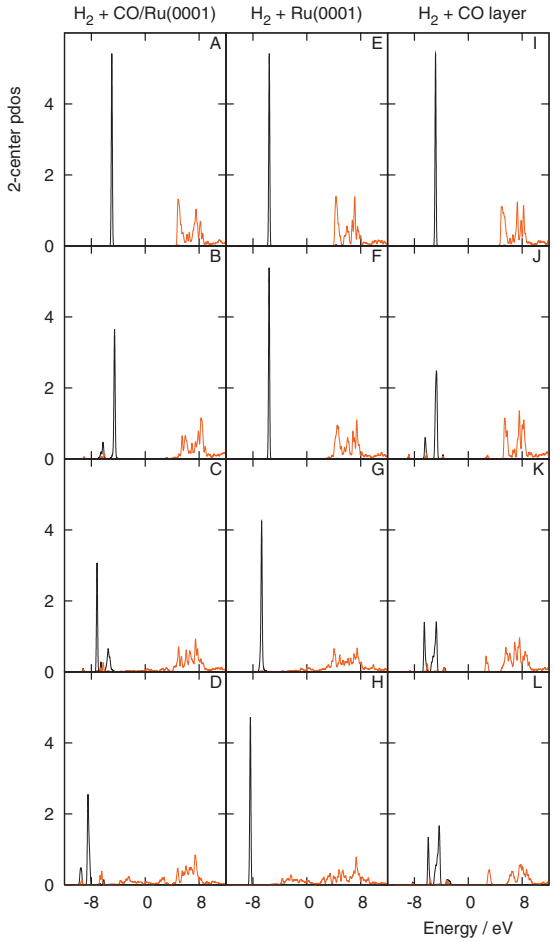

FIG. 6. Two-center PDOS (arb. units) for the full system, H_2 with the CO/Ru(0001) surface for four selected configurations (shown in Fig. 5) along one reaction path: (a) gas phase; (b) entrance channel; (c) barrier; and (d) first chemisorption minimum. Black: H_2 bonding state; red: H_2 antibonding state. The coordinates of the configurations are given in Table V. The Fermi level is set at zero energy. The same is shown for the H_2+Ru system [(f)–(h)], and the H_2+CO overlayer system [(i)–(l)].

6(j)], which is easily explained by the spatial extent of the occupied (surface-hybridized) CO orbitals: Both 4σ and 5σ are mainly extended along the CO bond axis (perpendicular to the surface), while the 1π orbitals are mainly extended parallel to the surface, creating larger overlaps with σ_g of the H_2 approaching the surface between the CO molecules.

When reaching the first barrier (configuration D) the picture is slightly more complicated. A large part of the repulsive energy of 0.29 eV for CO/Ru (Table V) appears to be due to the occupied-occupied repulsion between the H_2 σ_g orbital and the (surface-hybridized) CO 1π orbitals (0.24 eV, Table V). This is understood based on the above arguments. However, there is also a repulsive contribution from the interaction between the H_2 molecule and the Ru surface. Note, however, that if we take this contribution to be equal to the repulsive energy for H_2+CO/Ru minus that of H_2+CO (i.e., as 0.05 eV), then it appears to be smaller than one might expect based on the calculations of H_2 interacting with a clean Ru surface (0.14 eV, Table V). The fact that the barrier (0.29 eV) is smaller than the sum of the repulsive energies obtained for the H_2+CO and H_2+Ru subsystems (0.24 +0.14=0.38 eV, Table V) suggests an interpretation in which the Ru surface as a subsystem is (slightly) *more* reactive for this approach geometry *with* CO preadsorbed than *without* it. To explain this we need to consider the interaction of H_2 with the clean Ru surface in some detail. However, first we should note that we do not think the alternative explanation to be correct, that adsorbing CO onto the surface makes it *less* repulsive than the overlayer by itself. The reason is that the repulsion from the CO overlayer fully accounts for the repulsion on the approach to the barrier in H_2+CO/Ru (configurations B and C, Table V), since the energies for H_2 interacting with the CO/Ru(0001) and with the CO overlayer are almost the same. If adsorbing CO onto the surface makes it less repulsive than the overlayer by itself, we believe this would not have been the case.

In general, the height of the barrier to H_2 dissociation on top of a *d*-metal atom can, to a large extent, be understood as resulting from a competition between increasing overlap of the H_2 σ_u orbital and the metal d_{xz}-orbital (or a linear combination of d_{xz} and d_{yz} orbitals), decreasing overlap of the H_2 σ_g orbital and the metal d_{z^2}-orbital, and from the degree of occupation of the metal *d*-orbitals involved in the interactions (see, e.g., Ref. 88). In the case of H_2 approaching the clean Ru surface a part of the increase in the σ_g-d_{z^2} interaction can be seen from the shift of the σ_g peak to lower energy [Figs. 6(e)–6(g)]. This part of the σ_g-d_{z^2} interaction is molecule-surface bonding. However, since the *d*-band to a large degree is filled for Ru, there is a considerable population of the molecule-surface antibonding part from the same orbital interaction (this is not visible in Figs. 6(e)–6(g) because it has predominantly metal-*d* character and does not show up in the H_2 σ_g PDOS plots). The net effect of the σ_g-d_{z^2} interaction is therefore molecule-surface antibonding.

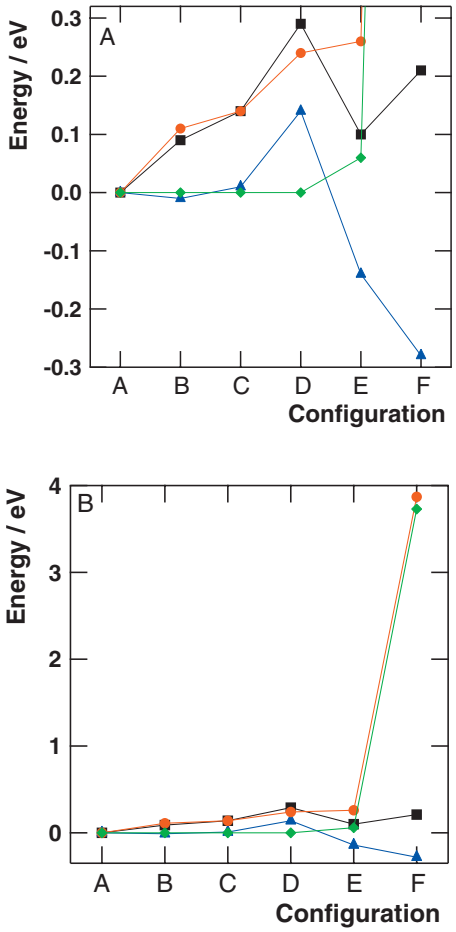

FIG. 7. Energy profiles for six selected configurations (shown in Fig. 5) along one reaction path of H_2 dissociation on CO-precovered Ru(0001). The gas phase energy is taken to be zero. The profiles are compared for H_2 +CO/Ru(0001) (black), H_2+Ru(0001) (blue), H_2 with the CO overlayer (red), and H_2 only (green). (Top panel) Plotted between −0.30 and 0.32 eV. (Bottom panel) Plotted between −0.35 and 4 eV. The coordinates of the configurations are given in Table V.

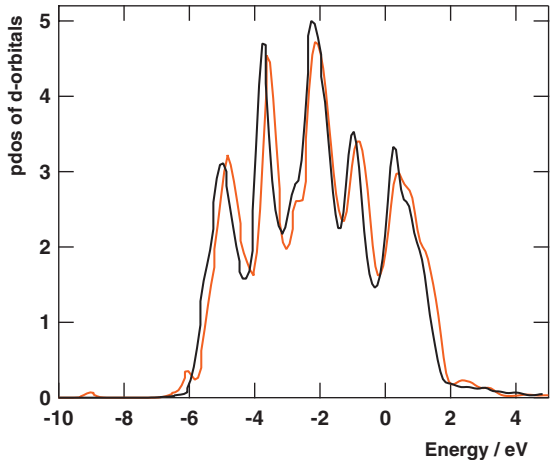

FIG. 8. The PDOS shows the *d*-orbitals with (red) and without (black) CO adsorbed on the surface. For the case of CO adsorbed on Ru, the PDOS is displayed for the *d*-orbitals on the free surface Ru atoms, i.e., the green Ru atoms in Fig. 4 above which the first barrier to dissociation is crossed.

The σ_u-d_{xz} interaction leads to a slight occupation of the H_2 σ_u orbital [Fig. 6(g)], as can be seen from the small bond elongation in Table V for configuration D. The interaction is molecule-surface bonding, but the occupation of the resulting orbitals is not large enough to counter the repulsive σ_g-d_{z^2} interaction. Thus, the net effect of the σ_g-d_{z^2} and σ_u-d_{xz} interactions is to create a barrier to H_2 dissociation along this path of 0.14 eV.

As already indicated, the numbers from Table V suggest that the contribution to the overall barrier of 0.29 eV from the Ru surface itself is only 0.05 eV. This is 0.09 eV lower than the corresponding barrier on clean Ru (note that the path considered is not exactly the MEP for the H_2+Ru system[68]). The reason can clearly be seen in Fig. 8: Upon CO adsorption the *d*-orbitals of the surface Ru atoms with no adsorbed CO on them show a clear (small) shift upwards with respect to the Fermi level (the *d*-orbitals of the surface Ru atoms with adsorbed CO on them show a downward shift as expected [results not shown]). This reduces the repulsion due to a smaller occupation of the molecule-surface antibonding part of the σ_g-d_{z^2} interaction. Although we here use a language from a localized molecular orbital interpretation picture, it is fully consistent with what would have been deduced from the much used *d*-band model: The center of the *d*-band of the reaction ensemble (i.e., the surface Ru atoms without adsorbed CO) moves upwards with respect to the Fermi level upon CO adsorption, and therefore the free surface metal atoms become more reactive.[89] It is important to stress that this discussion pertains to the Ru surface subsystem (and as such is rather academical, although interesting), the total effect of CO adsorption on the Ru surface is to increase the hydrogen dissociation barrier. The attribution of the weaker total repulsion to the Ru part of the system does not represent the only possible explanation of the effect, but the explanation we provide is backed up by an analysis of the underlying electronic structure with the *d*-band model.[89]

The reduction in repulsion moving from configuration D (the first barrier) to configuration E (first chemisorption well) is seen to be caused mainly by the attraction toward the Ru surface, as there is little change in the interaction with the CO overlayer from the barrier configuration [Table V, Figs. 6(k) and 6(l)]. This can be explained by the increasing population of the molecule-surface bonding molecular orbitals originating from the σ_u-d_{xy} interaction [Figs. 6(c), 6(d), 6(g), and 6(h)].

IV. CONCLUSIONS

We studied different reaction paths for the dissociative adsorption of hydrogen on a Ru(0001) surface precovered with 1/3 ML CO with DFT calculations. One reaction path was investigated in more detail by an energy decomposition analysis and by PDOS calculations.

The reaction path shows a complex energy landscape. The minimum barrier to dissociation is 0.29 eV. At this barrier, the H–H bond is hardly stretched. The system then moves to a molecular chemisorption minimum. Next, the molecule has to overcome a second barrier, which is lower than the first barrier of 0.29 eV. The existence of the second barrier is associated with the movement of one of the H atoms from a location near the top site toward the favored atomic chemisorption minimum, i.e., a site near an hcp site.

Behind this barrier a second local chemisorption minimum is present. To fully dissociate, the other H atom also moves to a site near an hcp site. To reach this position the molecule has to overcome a third barrier. The dissociation process is endoergic, as opposed to bare Ru(0001) where H_2 dissociation is exoergic.[68]

The height of the lowest first barrier to dissociation found from constrained 2D cuts (0.30 eV for the top site) compares very well to the one found from the ANEB calculations (0.29 eV), and the same is true for the barrier position. However, for this 2D cut no dissociation channel is observed. From the ANEB calculations it is clear that dissociation occurs after significant changes in the position of the COM of the H_2 molecule that reflect the consecutive movements of the individual H atoms to their favored chemisorption sites, these movements not being allowed in the 2D calculations where the COM is fixed. For the other high-symmetry sites studied higher barriers are found (0.74 eV for the t2f site and 0.85 eV for the bridge site). For dissociation above the hcp site very high energies are observed, indicating that this is not a favorable route to dissociation.

The presence of CO on the surface increases the barrier to dissociation compared with the barrier for bare Ru(0001) (from 0.085 eV for the MEP on bare Ru (Ref. 68) to 0.29 eV for CO/Ru(0001)). The results of the applied energy decomposition and molecular orbital analysis suggest that the increase in the barrier is mainly due to an occupied-occupied interaction between the bonding H_2 σ_g orbital and the (surface-hybridized) CO 1π orbitals. A small repulsive contribution to the barrier from the interaction between the H_2 molecule and the Ru part of the CO covered Ru surface is found, but it is smaller than one might expect based on the calculations of H_2 interacting with a clean Ru surface, and on calculations of H_2 interacting with the CO overlayer only. Counter to intuition, the analysis suggests that the Ru surface as a subsystem is (slightly) more reactive for the reaction path studied with CO preadsorbed than without it. Specifically, an upwards shift of the center of the *d*-band associated with the free surface Ru atoms in CO/Ru(0001), relative to that of bare Ru(0001), suggests that the free surface Ru atoms should be more reactive in CO/Ru(0001), and that this accounts for the smaller total repulsion. Thus, the results indicate that the influence of CO on H_2 dissociation on Ru is not only a simple site-blocking effect, the electronic structure of the underlying Ru (in particular the *d*-orbitals on the free Ru atoms) is also changed.

ACKNOWLEDGMENTS

The authors would like to thank M. C. van Hemert and M. F. Somers for help with the computer facilities, J. Chen for help with the projected density of states calculations, and G. P. Krishnamohan for help with the visualization of the reaction pathways. This research was facilitated by a PIONIER grant and a CW-ECHO grant from NWO for G.J.K.

[1] K. Christmann, Surf. Sci. Rep. **9**, 1 (1988).
[2] A. Gross, Surf. Sci. Rep. **32**, 291 (1998).
[3] G. J. Kroes, Prog. Surf. Sci. **60**, 1 (1999).
[4] G. J. Kroes, A. Gross, E. J. Baerends, M. Scheffler, and D. A. McCormack, Acc. Chem. Res. **35**, 193 (2002).
[5] G. J. Kroes and M. F. Somers, J. Theor. Comput. Chem. **4**, 493 (2005).
[6] T. H. Rod, A. Loggadottir, and J. K. Nørskov, J. Chem. Phys. **112**, 5343 (2000).
[7] J. A. Schwarz, Surf. Sci. **87**, 525 (1979).
[8] D. W. Goodman and M. Kishkinova, Surf. Sci. **105**, L265 (1981).
[9] S. Johnson and R. J. Madix, Surf. Sci. **108**, 77 (1981).
[10] M. Kiskinova and D. W. Goodman, Surf. Sci. **108**, 64 (1981).
[11] K. D. Rendulic, G. Anger, and A. Winkler, Surf. Sci. **208**, 404 (1989).
[12] M. L. Burke and R. J. Madix, Surf. Sci. **237**, 1 (1990).
[13] L. K. Verheij, M. B. Hugenschmidt, B. Poelsema, and G. Comsa, Catal. Lett. **9**, 195 (1991).
[14] J. K. Brown, A. C. Luntz, and P. A. Schultz, J. Chem. Phys. **95**, 3767 (1991).
[15] S. Wilke and M. Scheffler, Surf. Sci. **329**, L605 (1995).
[16] L. K. Verheij and M. B. Hugenschmidt, Surf. Sci. **324**, 185 (1995).
[17] S. Wilke and M. Scheffler, Phys. Rev. Lett. **76**, 3380 (1996).
[18] A. Gross, Appl. Phys. A: Mater. Sci. Process. **67**, 627 (1998).
[19] A. Gross, C. M. Wei, and M. Scheffler, Surf. Sci. **416**, L1095 (1998).
[20] C. M. Wei, A. Gross, and M. Scheffler, Phys. Rev. B **57**, 15572 (1998).
[21] P. A. Gravil and H. Toulhoat, Surf. Sci. **430**, 176 (1999).
[22] A. Gross and M. Scheffler, Phys. Rev. B **61**, 8425 (2000).
[23] A. T. Gee, B. E. Hayden, C. Mormiche, and T. S. Nunney, Surf. Sci. **512**, 165 (2002).
[24] E. D. L. Rienks, J. W. Bakker, A. Baraldi, S. A. C. Caribineiro, S. Lizzit, C. J. Weststrate, and B. E. Nieuwenhuys, J. Chem. Phys. **119**, 6245 (2003).
[25] S. A. C. Carabineiro, W. D. van Noort, and B. E. Nieuwenhuys, Surf. Sci. **532–535**, 96 (2003).
[26] A. R. Cholach, N. N. Bulgakov, and B. E. Nieuwenhuys, Surf. Sci. **573**, 264 (2004).
[27] H. Ueta, I. M. N. Groot, M. A. Gleeson, S. Stolte, G. C. McBane, L. B. F. Juurlink, and A. W. Kleyn, ChemPhysChem **9**, 2372 (2008).
[28] P. J. Feibelman and D. R. Hamann, Phys. Rev. Lett. **52**, 61 (1984).
[29] P. J. Feibelman and D. R. Hamann, Surf. Sci. **149**, 48 (1985).
[30] J. M. MacLaren, J. B. Pendry, and R. W. Joyner, Surf. Sci. **165**, L80 (1986).
[31] J. K. Nørskov, S. Holloway, and N. D. Lang, Surf. Sci. **137**, 65 (1984).
[32] B. Hammer, K. W. Jacobsen, and J. K. Nørskov, Surf. Sci. **297**, L68 (1993).
[33] M. Johansson, O. Lytken, and I. Chorkendorff, Surf. Sci. **602**, 1863 (2008).
[34] G. A. Mills and F. W. Steffgen, Catal. Rev. - Sci. Eng. **8**, 159 (1974).
[35] M. A. Vannice, J. Catal. **37**, 449 (1975).
[36] M. A. Vannice, Catal. Rev. - Sci. Eng. **14**, 153 (1976).
[37] T. E. Madey, D. W. Goodman, and R. D. Kelley, J. Vac. Sci. Technol. **16**, 433 (1979).
[38] H. H. Storch, N. Golumbic, and R. B. Anderson, *The Fischer-Tropsch and Related Syntheses* (Wiley, New York, 1951).
[39] M. A. Vannice, J. Catal. **50**, 228 (1977).
[40] P. Winslow and A. T. Bell, J. Catal. **94**, 385 (1985).
[41] J. C. Fuggle, T. E. Madey, M. Steinkilberg, and D. Menzel, Surf. Sci. **52**, 521 (1975).
[42] I. M. Ciobica, A. W. Kleyn, and R. A. van Santen, J. Phys. Chem. B **107**, 164 (2003).
[43] I. M. Ciobica and R. A. van Santen, J. Phys. Chem. B **107**, 3808 (2003).
[44] M. Gajdoš, A. Eichler, and J. Hafner, J. Phys.: Condens. Matter **16**, 1141 (2004).
[45] G. Michalk, W. Moritz, H. Pfnür, and D. Menzel, Surf. Sci. **129**, 92 (1983).
[46] M. Gierer, H. Bludau, H. Over, and G. Ertl, Surf. Sci. **346**, 64 (1996).
[47] J. J. Mortensen, Y. Morikawa, B. Hammer, and J. K. Nørskov, Z. Phys. Chem. **198**, 113 (1997).
[48] C. Stampfl and M. Scheffler, Phys. Rev. B **65**, 155417 (2002).
[49] J. S. McEwen and A. Eichler, J. Chem. Phys. **126**, 094701 (2007).
[50] J. C. Fuggle, M. Steinkilberg, and D. Menzel, Chem. Phys. **11**, 307 (1975).
[51] T. E. Madey, Surf. Sci. **79**, 575 (1979).
[52] E. D. Williams and W. Weinberg, Surf. Sci. **82**, 93 (1979).
[53] H. Pfnür, D. Menzel, F. M. Hoffmann, A. Ortega, and A. M. Bradshaw, Surf. Sci. **93**, 431 (1980).
[54] H. Pfnür and D. Menzel, Surf. Sci. **148**, 411 (1984).
[55] H. Pfnür and H. Heier, Ber. Bunsenges. Phys. Chem **90**, 272 (1986).
[56] H. Pfnür and D. Menzel, J. Chem. Phys. **79**, 2400 (1983).

[57] J. Braun, K. L. Kostov, G. Witte, and C. Wöll, J. Chem. Phys. **106**, 8262 (1997).
[58] M. Lindroos, H. Pfnür, P. Feulner, and D. Menzel, Surf. Sci. **180**, 237 (1987).
[59] P. Feulner and D. Menzel, Surf. Sci. **154**, 465 (1985).
[60] I. M. N. Groot, H. Ueta, M. J. T. C. van der Niet, A. W. Kleyn, and L. B. F. Juurlink, J. Chem. Phys. **127**, 244701 (2007).
[61] J. K. Vincent, R. A. Olsen, G. J. Kroes, M. Luppi, and E. J. Baerends, J. Chem. Phys. **122**, 044701 (2005).
[62] Y. K. Sun and W. H. Weinberg, Surf. Sci. **214**, L246 (1989).
[63] D. E. Peebles, J. A. Schreifels, and J. M. White, Surf. Sci. **116**, 117 (1982).
[64] C. H. Mak, A. A. Deckert, and S. M. George, J. Chem. Phys. **89**, 5242 (1988).
[65] R. L. C. Wang, H. J. Kreuzer, P. Jacob, and D. Menzel, J. Chem. Phys. **111**, 2115 (1999).
[66] B. Riedmüller, I. M. Ciobica, D. C. Papageorgopoulos, B. Berenbak, R. A. van Santen, and A. W. Kleyn, Surf. Sci. **465**, 347 (2000).
[67] B. Riedmüller, D. C. Papageorgopoulos, B. Berenbak, R. A. van Santen, and A. W. Kleyn, Surf. Sci. **515**, 323 (2002).
[68] M. Luppi, R. A. Olsen, and E. J. Baerends, Phys. Chem. Chem. Phys. **8**, 688 (2006).
[69] P. Hohenberg and W. Kohn, Phys. Rev. **136**, B864 (1964).
[70] W. Kohn and L. J. Sham, Phys. Rev. **140**, A1133 (1965).
[71] See: DACAPO, http://www.camp.dtu.dk/campos/dacapo/.
[72] B. Hammer, L. B. Hansen, and J. K. Nørskov, Phys. Rev. B **59**, 7413 (1999).
[73] E. Christoffersen, P. Stoltze, and J. K. Nørskov, Surf. Sci. **505**, 200 (2002).
[74] J. P. Perdew, J. A. Chevary, S. H. Vosko, K. A. Jackson, M. R. Pederson, D. J. Singh, and C. Fiolhais, Phys. Rev. B **46**, 6671 (1992).
[75] C. Díaz, E. Pijper, R. A. Olsen, H. F. Busnengo, D. J. Auerbach, and G. J. Kroes, Science **326**, 832 (2009).
[76] D. Vanderbilt, Phys. Rev. B **41**, 7892 (1990).
[77] H. J. Monkhorst and D. J. Pack, Phys. Rev. B **13**, 5188 (1976).
[78] H. Over, W. Moritz, and G. Ertl, Phys. Rev. Lett. **70**, 315 (1993).
[79] A. Stroppa and G. Kresse, New J. Phys. **10**, 063020 (2008).
[80] B. Hammer, Y. Morikawa, and J. K. Nørskov, Phys. Rev. Lett. **76**, 2141 (1996).
[81] F. Abild-Pedersen and M. P. Andersson, Surf. Sci. **601**, 1747 (2007).
[82] H. Pfnür, P. Feulner, H. A. Engelhardt, and D. Menzel, Chem. Phys. Lett. **59**, 481 (1978).
[83] H. Pfnür, P. Feulner, and D. Menzel, J. Chem. Phys. **79**, 4613 (1983).
[84] G. Henkelman and H. Jónsson, J. Chem. Phys. **113**, 9978 (2000).
[85] P. W. Atkins and R. S. Friedman, *Molecular Quantum Mechanics*, 3rd ed. (Oxford University Press, USA, 1997).
[86] See supplementary material at http://dx.doi.org/10.1063/1.3378278 for details of the other three reaction paths (reaction paths II–IV).
[87] K. Svensson, L. Bengtsson, J. Bellman, M. Hassel, M. Persson, and S. Andersson, Phys. Rev. Lett. **83**, 124 (1999).
[88] J. C. Chen, J. C. Juanes-Marcos, A. Al-Halabi, R. A. Olsen, and G. J. Kroes, J. Phys. Chem. C **113**, 11027 (2009).
[89] B. Hammer, Phys. Rev. B **63**, 205423 (2001).